Numerical Simulation in Applied Geophysics.
From the Mesoscale to the Macroscale

Juan E. Santos

CONICET, Instituto del Gas y del Petróleo, Facultad de Ingeniería, UBA y UNLP.

Department of Mathematics, Purdue University. ARGENTINA y USA.

Patricia M. Gauzellino

Depto. Geofísica Aplicada, Facultad de Cs. Astr. y Geofísicas, UNLP. ARGENTINA.

Gabriela B. Savioli

Instituto del Gas y del Petróleo, Facultad de Ingeniería, UBA. ARGENTINA.

Robiel Martínez Corredor

Facultad de Ingeniería, UNLP. ARGENTINA.

ABSTRACT

This paper presents a collection of finite element procedures to model seismic wave propagation at the macroscale taking into account the effects caused by heterogeneities occuring at the mesoscale. For this purpose we first apply a set of compressibility and shear experiments to representative samples of the heterogeneous fluid saturated material. In turn these experiments yield the effective coefficients of an anisotropic macroscopic medium employed for numerical simulations at the macroscale. Numerical experiments illustrate the implementation of the proposed methodology to model wave propagation at the macroscale in a patchy brine-CO_2 saturated porous medium containing a dense set of parallel fractures.

Keywords: poroelasticity, anisotropy, fractures, finite elements, numerical upscaling.

1. INTRODUCTION

Seismic wave propagation is a common technique used in hydrocarbon exploration geophysics, mining and reservoir characterization and production. The subsurface rocks can be considered as fluid-saturated poroviscoelastic media where local variations in the fluid and solid matrix properties, fine layering, fractures and craks at the mesoscale (on the order of centimeters) cause attenuation, dispersion and anisotropy of the seismic waves observed at the macroscale. These effects take place due to the balance of wave-induced fluid pressure gradients via a slow-wave diffusion process [1, 2, 3, 4].

To properly represent these type of mesoscopic-scale heterogeneities it would be necessary to use extremely fine meshes with the numerical simulations becoming very expensive or even not feasible. As an approach to solve this problem we suggest to perform numerical upscaling procedures to determine the complex and frequency dependent stiffness at the macroscale of an equivalent viscoelastic medium including the mesoscopic-scale effects. White et al. [5] and Saenger et al. [6] introduced the mesoscopic-loss mechanism in the framework of Biot theory. For fine layered poroelastic materials, the theories of Gelinsky and Shapiro [7] and Krzikalla and Müller [8] allow to obtain the stiffnesses of the equivalent anisotropic medium. In the case of determining equivalent effective media for fractured rocks, the works of Grechka and Kachanov [9, 10] can be referenced among others.

In this paper we present a numerical procedure to model mesoscopic effects in saturated porous media affecting the seismic observations at the macroscale.

First we employ a numerical upscaling procedure to obtain the five complex stiffnesses of an effective transversely isotropic medium with vertical axis of symmetry (VTI). The experiments describe the case of a dense set of horizontal fractures in a fluid-saturated poroelastic medium that behaves as a VTI medium when the average fracture distance is much smaller than the predominant wavelength of the traveling waves. These numerical experiments offer a alternative to laboratory measurements with the advantages that they are inexpensive, repeatable and essentially free from experimental errors. In addition, they may easily be run using alternative models of the rock and fluid properties and the physical process of wave propagation can be inspected during the experiment.

We use the Finite Element Method (FEM) to solve Biot equation of motion in the space-frequency domain with boundary conditions representing compressibility and shear harmonic experiments. A similar methodology had been applied in [11, 12, 13] to layered viscoelastic and poroelastic materials. Second a parallelizable iterative domain decomposition FEM is employed to describe wave propagation at the macroscale. The organization of the paper is as follows. Section 2 describes the suitable differential model to represent mesoscopic effects using theory of Biot. Section 3 presents the different harmonic experiments to determine the stiffness coefficients, while Section 4 shows numerical simulations that illustrate frequency and angular variations of velocity and attenuation of seismic waves in patchy brine-CO_2 saturated horizontally fractured samples. Section 5 presents the results of the seismic modeling in the macroscale obtained using a parallelizable procedure based in a nonconforming FE space. Finally, Section 6 provides some conclusions.

2. EQUATIONS OF BIOT AND EQUIVALENT MEDIUM

We consider fine isotropic fluid-saturated poroelastic layers. Let $u = (u^s(x), u^f(x))$ be the time Fourier transform of the displacement vector of the solid and fluid relative to the solid frame, respectively. Also let $\sigma_{kl}(u), p_f(u)$ denote the Fourier transform of the total stress and the fluid pressure, respectively.

On each plane layer n in a sequence of N layers, the frequency-domain stress-strain relations are

$$\sigma_{kl}(u) = 2\mu\,\varepsilon_{kl}(u^s) + \delta_{kl}\left(\lambda_G\,\nabla \cdot u^s + \alpha M \nabla \cdot u^f\right),$$
$$p_f(u) = -\alpha M \nabla \cdot u^s - M \nabla \cdot u^f.$$

being μ the shear modulus of the material and $\varepsilon_{kl}(u^s)$ the strain tensor of the solid. In addition, $\lambda_G = K_G - 2\mu/3$, where K_G is the bulk modulus of the saturated material, the effective stress coefficient is $\alpha = 1 - K_m/K_s$ with K_m and K_s denote the bulk modulus of the dry matrix and the solid grains composing the solid matrix, respectively. Also, the coefficient M is determined from the relation

$$M = \frac{K_s K_f}{K_f(\alpha - \phi) + K_s \phi},$$

where K_f is the bulk modulus of the saturant fluid and ϕ is the porosity. See [4].

In the diffusive range of frequencies the Biot's equations are

$$\nabla \cdot \sigma(u) = 0,$$
$$i\omega\frac{\eta}{\kappa}u^f(x,\omega) + \nabla p_f(u) = 0,$$

where ω is the angular frequency, η the fluid viscosity and κ the frame permeability.

As the considered medium behaves as a VTI medium, let $\tau_{\mathbf{ij}}$ denotes the stress tensor of this equivalent medium at the macroscale. The corresponding stress-strain relations, stated in the space-frequency domain, for a closed system where the variation of fluid content is zero, i.e. $\nabla \cdot u^f = 0$, are:

$$\tau_{11}(u) = p_{11}\,\epsilon_{11}(u^s) + p_{12}\,\epsilon_{22}(u^s) + p_{13}\,\epsilon_{33}(u^s),$$
$$\tau_{22}(u) = p_{12}\,\epsilon_{11}(u^s) + p_{11}\,\epsilon_{22}(u^s) + p_{13}\,\epsilon_{33}(u^s),$$
$$\tau_{33}(u) = p_{13}\,\epsilon_{11}(u^s) + p_{13}\,\epsilon_{22}(u^s) + p_{33}\,\epsilon_{33}(u^s),$$
$$\tau_{23}(u) = 2\,p_{55}\,\epsilon_{23}(u^s),$$
$$\tau_{13}(u) = 2\,p_{55}\,\epsilon_{13}(u^s),$$
$$\tau_{12}(u) = 2\,p_{66}\,\epsilon_{12}(u^s).$$

This approach provides the complex velocities of the fast modes and takes into account interlayer flow effects.

3. HARMONIC EXPERIMENTS

To determine the complex stiffness coefficients we solve a set of boundary value problems (BVPs) for the Biot's equation in the frequency-domain using the FEM. This procedure was presented and validated in [13].

For the 2D case, on a reference square $\Omega = (0, L)^2$ with boundary Γ in the (x_1, x_3)-plane. We stand for $\Gamma = \Gamma^L \cup \Gamma^B \cup \Gamma^R \cup \Gamma^T$, where

$$\Gamma^L = \{(x_1, x_3) \in \Gamma : x_1 = 0\},$$
$$\Gamma^R = \{(x_1, x_3) \in \Gamma : x_1 = L\},$$
$$\Gamma^B = \{(x_1, x_3) \in \Gamma : x_3 = 0\},$$
$$\Gamma^T = \{(x_1, x_3) \in \Gamma : x_3 = L\}.$$

The sample is subjected to harmonic compressibility and shear tests described by the following sets of boundary conditions (BCs).

$$p_{33(\omega)}:$$

The BCs are:

$$\sigma(u)\nu \cdot \nu = -\Delta P, \quad (x_1, x_3) \in \Gamma^T,$$
$$\sigma(u)\nu \cdot \chi = 0, \quad (x_1, x_3) \in \Gamma,$$
$$u^s \cdot \nu = 0, \quad (x_1, x_3) \in \Gamma^L \cup \Gamma^R \cup \Gamma^B,$$
$$u^f \cdot \nu = 0, \quad (x_1, x_3) \in \Gamma,$$

where ν is the unit outer normal on Γ and χ is a unit tangent on Γ so that $\{\nu, \chi\}$ is an orthonormal system on Γ.

Denote by V the original volume of the sample and by $\Delta V(\omega)$ its (complex) oscillatory volume change. In the quasistatic case,

$$\frac{\Delta V(\omega)}{V} = -\frac{\Delta P}{p_{33}(\omega)}.$$

Then after computing the average $u_3^{s,T}(\omega)$ of the vertical displacements on Γ^T, we approximate

$$\Delta V(\omega) \approx L u_3^{s,T}(\omega)$$

which enable us to compute $p_{33}(\omega)$.

$p_{11}(\omega)$:

To determine $p_{11}(\omega)$ we solve an identical boundary value problem than for p_{33} but for a 90° rotated sample.

$p_{55}(\omega)$:

The BCs are:

$$-\sigma(u)\nu = g, \quad (x_1, x_3) \in \Gamma^T \cup \Gamma^L \cup \Gamma^R,$$
$$u^s = 0, \quad (x_1, x_3) \in \Gamma^B,$$
$$u^f \cdot \nu = 0, \quad (x_1, x_3) \in \Gamma,$$

where

$$g = \begin{cases} (0, \Delta G), & (x_1, x_3) \in \Gamma^L, \\ (0, -\Delta G), & (x_1, x_3) \in \Gamma^R, \\ (-\Delta G, 0), & (x_1, x_3) \in \Gamma^T. \end{cases}$$

The change in shape suffered by the sample is

$$\tan[\theta(\omega)] = \frac{\Delta G}{p_{55}(\omega)},$$

where $\theta(\omega)$ is the angle between the original positions of the lateral boundaries and the location after applying the shear stresses. Since $\tan[\theta(\omega)] \approx u_1^{s,T}(\omega)/L$, where $u_1^{s,T}(\omega)$ is the average horizontal displacement at Γ^T, $p_{55}(\omega)$ can be determined.

$p_{66}(\omega)$:

To determine $p_{66}(\omega)$ (shear waves traveling in the (x_1, x_2)-plane), we rotate the layered sample 90° and apply the shear test as indicated for $p_{55}(\omega)$.

$p_{13}(\omega)$:

The BCs are:

$$\sigma(u)\nu \cdot \nu = -\Delta P, \quad (x_1, x_3) \in \Gamma^R \cup \Gamma^T,$$
$$\sigma(u)\nu \cdot \chi = 0, \quad (x_1, x_3) \in \Gamma,$$
$$u^s \cdot \nu = 0, \quad (x_1, x_3) \in \Gamma^L \cup \Gamma^B,$$
$$u^f \cdot \nu = 0, \quad (x_1, x_3) \in \Gamma.$$

In this experiment $\epsilon_{22} = \nabla \cdot u^f = 0$, so that

$$\tau_{11} = p_{11}\epsilon_{11} + p_{13}\epsilon_{33}, \quad \tau_{33} = p_{13}\epsilon_{11} + p_{33}\epsilon_{33},$$

where $\epsilon_{11}, \epsilon_{33}$ are the strain components at the right lateral side and top side of the sample, respectively. Then, since in this experiment

$$\tau_{11} = \tau_{33} = -\Delta P,$$

$$p_{13}(\omega) = (p_{11}\epsilon_{11} - p_{33}\epsilon_{33}) / (\epsilon_{11} - \epsilon_{33}).$$

4. NUMERICAL RESULTS AT THE MESOSCALE

In order to illustrate the procedure we consider a brine-CO2 patchy saturated material with fractures. We choose our representative sample at the mesoscale as a square of 160 cm side length with 10 periods of 1 cm fracture, 15 cm background. This sample is characterized by a porosity $\phi = 0.25$ in the background and $\phi = 0.5$ in the fractures. The grain density is $\rho_s = 2650$ kg/m^3, while $K_s = 37$ GPa and $\mu_s = 44$ GPa are the bulk and shear moduli, respectively. Using the Krief model [14] we obtain $K_m = 1.17$ GPa and $\mu = 1.4$ GPa for the dry bulk and shear modulus of the background and $K_m = 0.58$ GPa and $\mu = 0.68$ GPa for the fractures. Permeability is obtained as $\kappa = r_g^2 \phi^3 / (45 - 45\phi)^2$ [15], where $r_g = 20$ μm is the average radius of the grains. The discrete boundary value problems to determine the complex stiffnesses $p_{IJ}(\omega)$ at the macroscale are solved for 30 frequencies using a public domain sparse matrix solver package.

Using relations given in [4] it is possible to determine the energy velocities and dissipation coefficients from the $p_{IJ}(\omega)$. The complex velocities of the equivalent VTI anisotropic medium are [4]

$$v_{qP} = (2\bar{\rho})^{-1/2}\sqrt{p_{11}l_1^2 + p_{33}l_3^2 + p_{55} + A},$$
$$v_{qSV} = (2\bar{\rho})^{-1/2}\sqrt{p_{11}l_1^2 + p_{33}l_3^2 + p_{55} - A},$$
$$A = \sqrt{[(p_{11} - p_{55})l_1^2 + (p_{55} - p_{33})l_3^2]^2 + 4[(p_{13} + p_{55})l_1 l_3]^2},$$

where $\bar{\rho} = \langle \rho \rangle$ is the thickness weighted average of the bulk density, $l_1 = \sin\theta$ and $l_3 = \cos\theta$ are the directions cosines, θ is the propagation angle between the wavenumber vector and the x_3-symmetry axis and the two velocities correspond to the qP and qSV waves, respectively. The seismic phase velocity and quality factors are given by

$$v_p = \left[\text{Re}\left(\frac{1}{v}\right)\right]^{-1} \quad \text{and} \quad Q = \frac{\text{Re}(v^2)}{\text{Im}(v^2)},$$

where v represents either v_{qP} or v_{qSV}.

The energy-velocity vector $\mathbf{v}_e$ of the qP and qSV waves is

$$\frac{\mathbf{v}_e}{v_p} = (l_1 + l_3 \cot\psi)^{-1}\hat{\mathbf{e}}_1 + (l_1 \tan\psi + l_3)^{-1}\hat{\mathbf{e}}_3,$$

with ψ being the angle between the energy-velocity vector and the x_3-axis.

Figures 1, 2 display polar representations of the qP and qSV energy velocity vectors at 50 Hz, respectively, where it can be observed the anisotropy induced by fractures. Figure 3 shows the dissipation factor of the qP waves at 50 Hz,
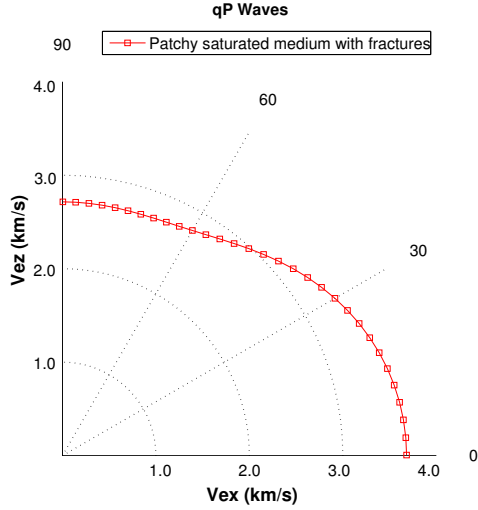
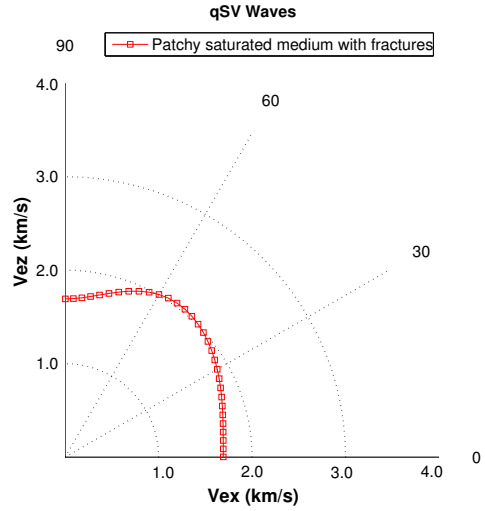Figure 1: Polar representation of the qP energy velocity vector at 50 Hz

Figure 2: Polar representation of the qSV energy velocity vector at 50 Hz

where it is seen that energy losses are much higher for angles between 60 and 90 degrees, i.e., for waves traveling in the direction incident normal to the fracture layering. Notice that for qP waves dissipation anisotropy is much important than velocity anisotropy.

Figure 4 shows the fluid pressure distribution at 50 Hz for compressions normal to the fracture layering (p_{33} experiment), where it can be observed that pressure gradients take their highest values at the fractures.

5. NUMERICAL RESULTS AT THE MACROSCALE

We solve the following boundary value problem at the macroscale (in the domain Ω and boundary $\partial\Omega$):

$$-\omega^2\rho u - \nabla \cdot \tau(u) = F, \quad \Omega$$
$$-\tau(u)\nu = i\omega\mathcal{D}u, \quad \partial\Omega,$$
$$\text{(absorbing bounday condition, } \mathcal{D} > 0)$$

where $u = (u_x, u_z)$ represents the displacement vector, ρ denotes the average density and $\tau(u)$ is the stress-tensor of our equivalent viscoelastic material, defined in terms of the calculated $p'_{IJ}s$ in the previous section using the upscaling procedure. Instead of solving the global problem associated with the above model, we obtain the solution using an iterative parallelizable hybridized domain decomposition procedure employing a nonconforming FE space. One of the main advantages of using nonconforming elements to solve wave propagation phenomena is that the amount of information exchanged among processors in a domain decomposition iterative
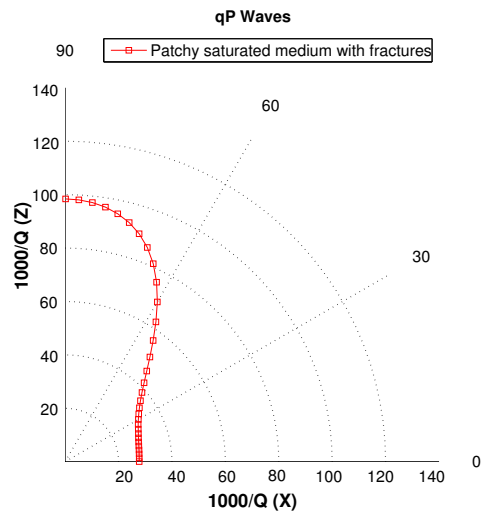

Figure 3: Polar representation of the dissipation factor for qP waves at 50 Hz
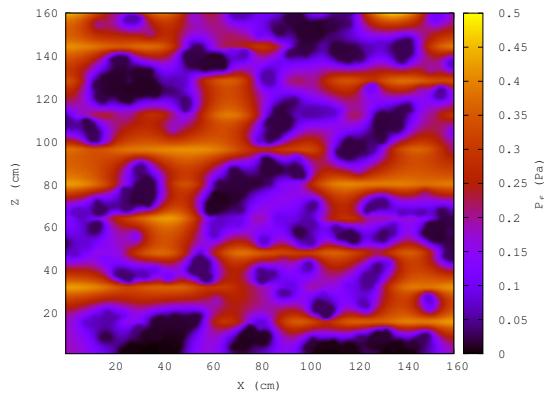
Figure 4: Fluid pressure distribution at 50 Hz for the compressibility test for p_{33} with compression normal to the fracture layering.

Figure 5: Snapshot of the vertical displacement at 100 ms.

procedure is considerable reduced as compared to the case when conforming elements are employed [16]. Another property of the nonconforming elements is that it is possible to obtain an estimate on the speed of convergence of the iterative domain decomposition procedure as a function of the mesh size h [17]. Moreover, it was shown in [18] that employing this nonconforming FE space allows to almost halves the number of points per wavelength necessary to reach a given accuracy as compared with conforming elements of the same degree of accuracy. The scalability of the algorithm was verified in [19]. Therefore, the algorithm is specially suited to solve large scale geophysical problems.

The computational model consists of a VTI homogeneous square medium and the source is a dilatational perturbation of central frequency at 30 Hz, located at the center of the domain. The mesh consists of 280 square cells having side length 3.57 m.

Figure 5 shows a snapshot of the vertical component of the displacement at 100 ms where the wavefront associated with the qP wave (fastest wavefront) and qSV wave (slowest wavefront) are clearly observed. The curvature of the wavefronts are a measure of the degree of the anisotropy of the medium.

6. CONCLUSIONS

This paper presents a methodology to model seismic wave propagation in highly heterogeneous fluid saturated porous materials. The examples demonstrate the capability of the upscaling finite element experiments performed at the mesoscale to determine the anisotropic coefficients in the constitutive relations of an equivalent viscoelastic medium at the macroscale. In particular we have shown that the presence of fractures in-
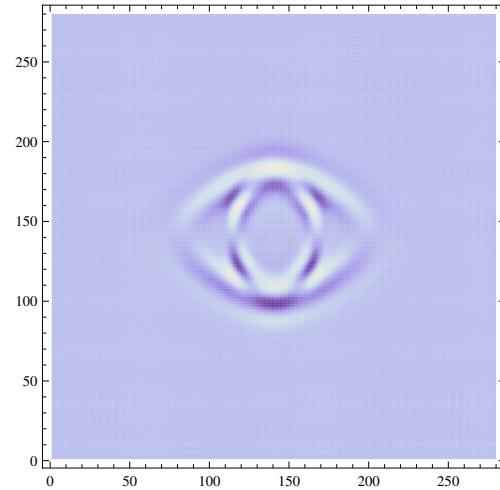
duces strong velocity and attenuation anisotropy that can be observed at the macroscale. Finally, we stand out the techniques presented here to model acoustics of porous media can be extended to other fields, like ultrasound testing of quality of foods, groundwater flow and contamination among others.

7. REFERENCES

[1] M.A. Biot, "Theory of propagation of elastic waves in a fluid-saturated porous solid. I. Low frequency range", *J. Acoust. Soc. Amer.*, Vol. 28, 1956, pp. 168-171.

[2] M.A. Biot, "Theory of propagation of elastic waves in a fluid-saturated porous solid. II. High frequency range", *J. Acoust. Soc. Amer.*, Vol. 28, 1956, pp. 179-191.

[3] M.A. Biot, "Mechanics of deformation and acoustic propagation in porous media", *J. Appl. Phys.*, Vol. 33, 1962, pp. 1482-1498.

[4] J.M. Carcione, *Wave fields in real media: Wave propagation in anisotropic, anelastic and porous media*, in Handbook of Geophysical Exploration, 2nd edn , Oxford: Elsevier, 2007.

[5] J.E. White, N.G. Mikhaylova, F.M. Lyakhovitskiy "Low-frequency seismic waves in fluid saturated layered rocks", *Physics of the Solid Earth*, Vol. 11, 1975, pp. 654-659.

[6] E.H. Saenger, R. Ciz, O.S. Krüger, S.M. Schamalholz, B. Gurevich, S.A. Shapiro "Finite-difference modeling of wave propagation on microscale: A snapshot of the work

in progress", *Geophysics*, Vol. 72, 2007, pp. SM293-SM300.

[7] S. Gelinsky, S.A. Shapiro "Poroelastic Backus-averaging for anisotropic, layered fluid and gas saturated sediments", *Geophysics*, Vol. 62, 1997, pp. 1867-1878.

[8] F. Krzikalla, T. Müller "Anisotropic P-SV-wave dispersion and attenuation due to interlayer flow in thinly layered porous rocks", *Geophysics*, Vol. 76, 2011, pp. W-135.

[9] V. Grechka, M. Kachanov "Effective elasticity of rocks with closely spaced and intersecting cracks", *Geophysics*, Vol. 71, 2006, pp. D85-D91.

[10] V. Grechka, M. Kachanov "Effective elasticity of fractured rocks: A snapshot of the work in progress", *Geophysics*, Vol. 71, 2006, pp. W45-W58.

[11] S. Picotti, J.M. Carcione, J. Santos, D. Gei "Q-anisotropy in finely-layered media", *Geophys. Res. Lett.*, Vol. 37, 2010, pp. L06302.

[12] J. Santos, J.M. Carcione, S. Picotti "Viscoelastic-stiffness tensor of anisotropic media from oscillatory numerical experiments", *Comput. Methods Appl. Mech. Engrg.*, Vol. 200, 2011, pp. 896-904.

[13] J.M. Carcione, J. Santos, S. Picotti "Anisotropic poroelasticity and wave-induced fluid flow. Harmonic finite-element simulations", *Geophysics Journal International*, Vol. 186, 2011, pp. 1245-1254.

[14] M. Krief, J. Garat, J. Stellingwerff, J. Ventre "A petrophysical interpretation using the velocities of P and S waves (full waveform sonic)", *The Log Analyst*, Vol. 31, 1990, pp. 355-369.

[15] J.M. Carcione, B. Gurevich, F. Cavallini "A generalized Biot-Gassmann model for the acoustic properties of shaley sandstones", *Geophys. Prosp.*, Vol. 48, 2000, pp. 539-557.

[16] P. Gauzellino, J. Santos "Frequency domain wave propagation modeling in exploration seismology", *Journal of Computational Acoustics*, Vol. 9, 2001, pp. 941-955.

[17] T. Ha, J. Santos, D. Sheen "Nonconforming finite element methods for the simulation of waves in viscoelastic solids", *Comput. Methods Appl. Mech. Engrg*, Vol. 191, 2002, pp. 5647-5670.

[18] F. Zyserman, P. Gauzellino, J. Santos "Dispersion analysis of a nonconforming finite element method for the Hemholtz and elastodynamic equations", *International Journal for Numerical Methods in Engineering*, Vol. 58, 2003, pp. 1381-1395.

[19] P. Gauzellino, F. Zyserman, J. Santos "Nonconforming finite element methods for the three-dimensional Helmholtz equation: iterative domain decomposition or global solution ?", *Journal of Computational Acoustics*, Vol. 17, 2009, pp. 159-174.